frontiers | Frontiers in Materials

TYPE Original Research
PUBLISHED 09 September 2022
DOI 10.3389/fmats.2022.1016820

OPEN ACCESS

EDITED BY
Jianlei Wang,
Chinese Academy of Sciences (CAS), China

REVIEWED BY
Xu Zhang,
Jiangnan University, China
Hongli Mao,
Nanjing Tech University, China
Yu Wang,
Changchun Institute of Applied Chemistry (CAS), China

*CORRESPONDENCE
Chen Zhang,
zc_jlu@hotmail.com

SPECIALTY SECTION
This article was submitted to Polymeric and Composite Materials, a section of the journal Frontiers in Materials

RECEIVED 11 August 2022
ACCEPTED 23 August 2022
PUBLISHED 09 September 2022

CITATION
Liang H, Fu G, Liu J, Tang Y, Wang Y, Chen S, Zhang Y and Zhang C (2022), A 3D-printed Sn-doped calcium phosphate scaffold for bone tissue engineering.
Front. Mater. 9:1016820.
doi: 10.3389/fmats.2022.1016820

A 3D-printed Sn-doped calcium phosphate scaffold for bone tissue engineering

Hong Liang[1], Gaosheng Fu[2], Jinrui Liu[1], Yueting Tang[1], Yujue Wang[1], Shan Chen[1], Yanjie Zhang[1] and Chen Zhang[1,2]*

[1]School of Materials and Chemistry Engeering, School of Geography and Oceanography, Minjiang University, Fuzhou, China, [2]Industrial Design Institute, Minjiang University, Fuzhou, China

Recent developments in 3D printing technology have been applied in the field of tissue engineering to fabricate customized bone repair scaffolds. β-tricalcium phosphate (β-TCP) is a bioceramic material with excellent potential as a scaffold foundation. Doping metallic ions with β-TCP will significantly enhance the mechanical property and bone regeneration performance compared with pure β-TCP specimens. In this study, we proposed a protocol for the fabrication of a Sn-doped β-TCP (Sn@TCP) scaffold using 3D printing technology, and the effect of Sn-doping on the physicochemical properties of the material and its *in vitro* bioactivity were investigated. Polyethylene glycol and polyvinyl alcohol were used as binder to construct Sn@TCP scaffolds which have good biocompability and can break down into H_2O and CO_2 after scaffolds sintering. The appearance of the scaffold constructed by 3D printing technology closely matched the computer design. The incorporation of Sn into β-TCP improved the compressive strength of the scaffold. Moreover, the Sn@TCP scaffold retained the inherently good biocompatibility of β-TCP and exhibited better osteoinduction capability than pure β-TCP scaffolds. Notably, the osteoinduction ability of Sn@TCP scaffolds were dependent on the Sn content. In conclusion, the 3D printing of Sn@TCP scaffolds with enhanced mechanical properties and osteoblast-inducing activity show great promise as scaffold materials in bone tissue engineering applications.

KEYWORDS

β-tcp, Sn-doping, 3D printing, mechanical properties, osteogenic induction

Introduction

In many instances, patients can develop bone defects due to injury, congenital diseases, and tumors. In these cases, bone substitutes are needed to fill and repair the defects (Grado et al., 2018). In the 1980s, calcium phosphate cements (CPCs) emerged as the first bone substitute materials. Since then, CPCs have been employed as injectable biomaterials in synthetic bone substitutes because of their excellent osteocompatibility with the apatite mineral component of human bone and ease of use (Petre et al., 2019). In addition, β-TCP has shown to be a bioresorbable ceramic

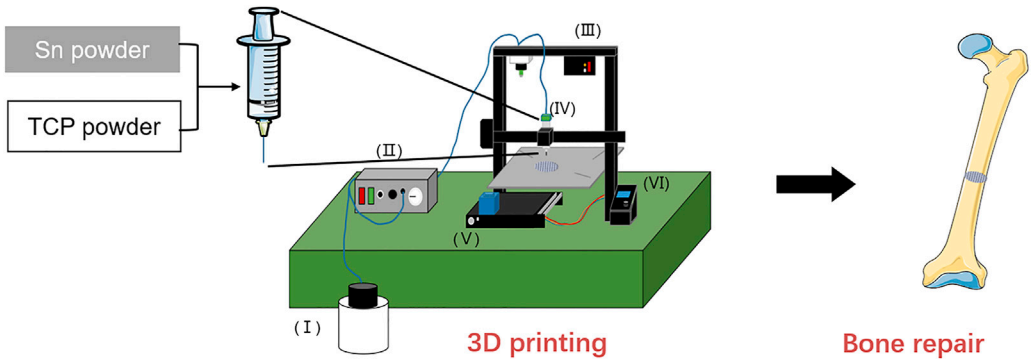

FIGURE 1
Schematic illustration of the preparation for Sn doping TCP scaffolds. Structure composition of 3D printer, I: Compressor, II: controller of compressor, III: pressure alarm, IV: printhead, V: *z*-axis screw, VI: controller of printing.

for bone tissue regeneration. For decades, β-TCP has been investigated as a potential scaffolding material for bone tissue engineering due to its biocompatibility, controlled bioactivity, and resorption/solubilization stability. Furthermore, it is physicochemically and structurally similar to natural bone (Vollmer et al., 2015; Kang et al., 2020).

In recent studies, doping of β-TCP with metallic ions, such as titanium (Ti), zinc (Zn) and magnesium (Mg) with β-TCP, showed

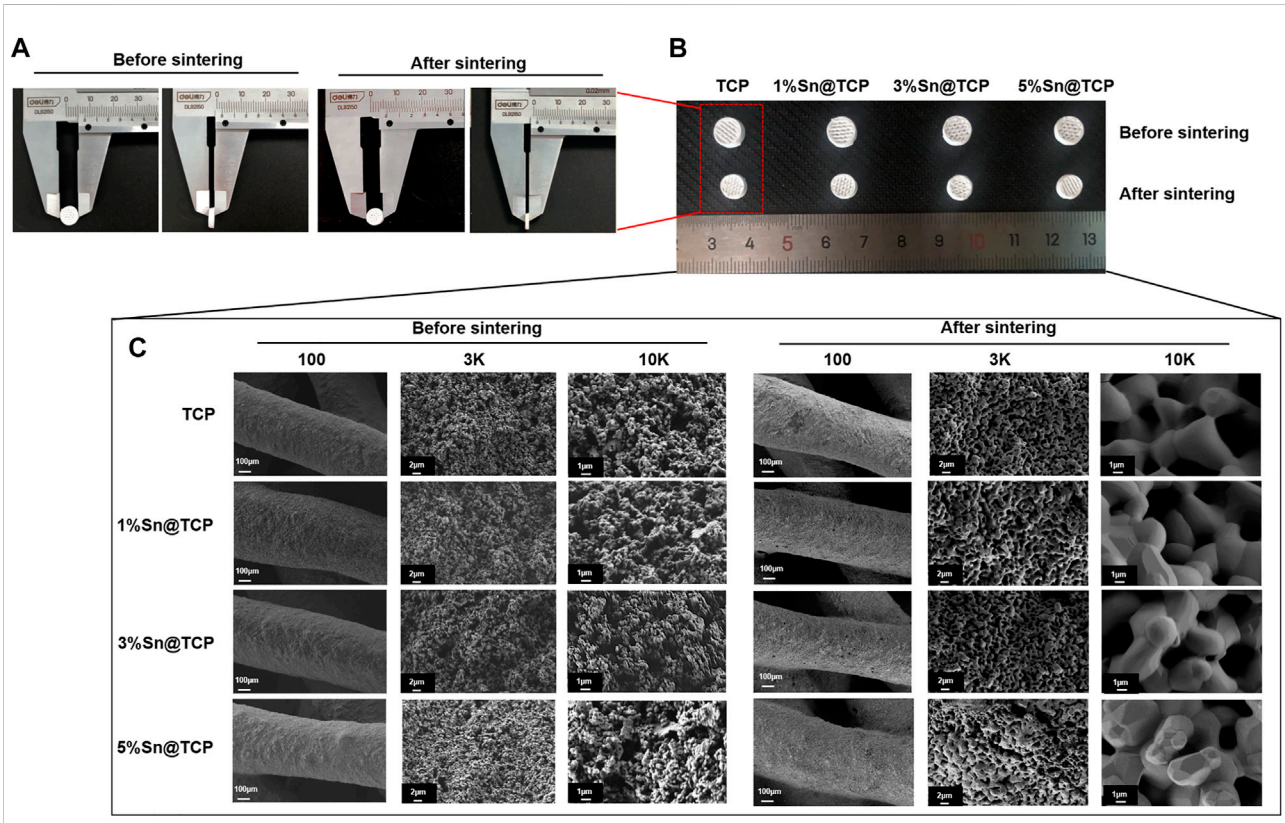

FIGURE 2
Morphology and structure of β-TCP (TCP) and Sn@TCP scaffolds. **(A–B)** The diameter and height of scaffolds before and after sintering. **(C)** SEM morphology of TCP, 1%Sn@TCP, 3%Sn@TCP and 5%Sn@TCP before and after sintering (Magnification from 100 to 10K, bar = 100 μm, 2μm, and 1 μm).

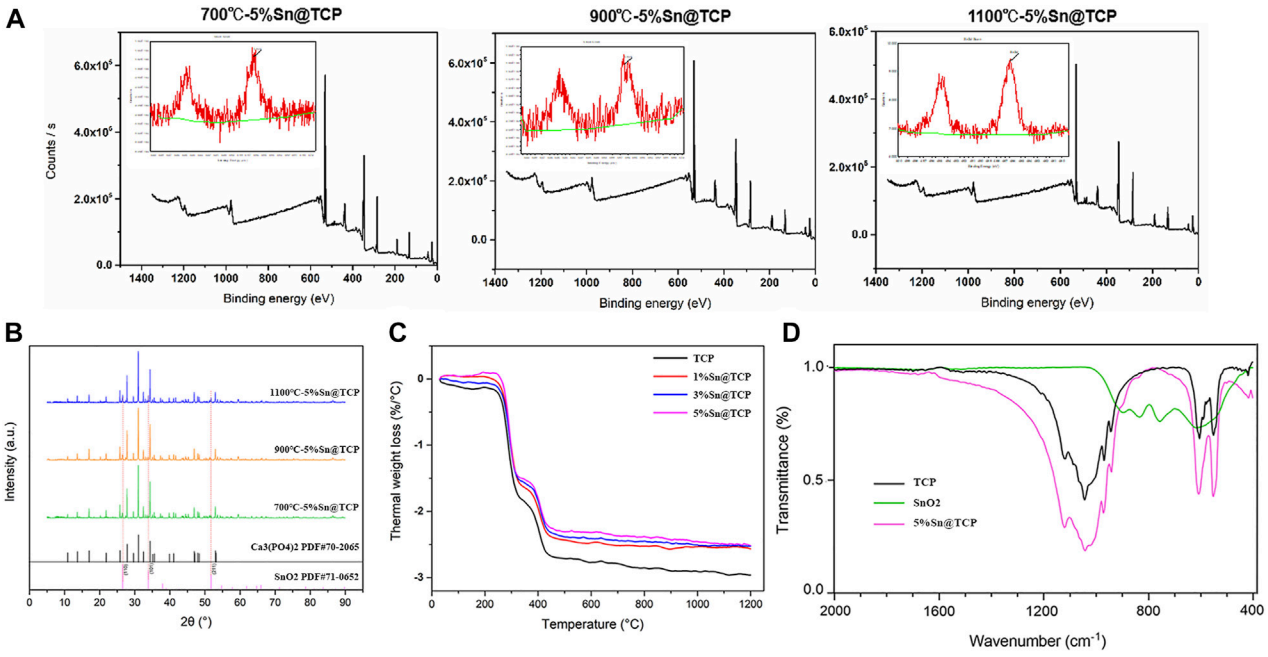

FIGURE 3
Characterization of TCP powders with different Sn doping. **(A)** XPS spectra of 5%Sn@TCP with different sintering temperature (700°C, 900°C and 1,100°C). **(B)** XRD pattern of 5%Sn@TCP with different sintering temperature (700°C, 900°C and 1,100°C). **(C)** TG-DSC curves of TCP powders with different Sn doping after 1,100°C sintering. **(D)** FT-IR spectra of TCP, SnO_2 and 5%Sn@TCP powders.

significantly better bone regeneration than pure β-TCP specimens (Samanta et al., 2019). The incorporation of Mn into β-TCP improved the physicochemical properties and bilineage bioactivities (Deng et al., 2017). Tin (Sn) is one of the most essential trace elements in the human body and is shown to promote tissue growth (Nagy et al., 2000; Tao and Zhang, 2003; Lynch and Duckworth, 2020). Sn-based alloys, such as Mg-Sn alloys, Ti-Nb-Sn alloy, and Mg-Sn alloys combined with biphasic calcium phosphate ceramic (HA+β-TCP). These Sn-based alloys exhibit strength, creep resistance, and biocompatibility. They have been widely employed in biomedical applications involving different parts of the human body, including bone tissue implants and dental implants (Kubasek et al., 2013; Shuai et al., 2016; Wang et al., 2015). Therefore, Sn-doped β-TCP scaffolds may improve the compressive strength of bone and promote osteogenesis. However, to our knowledge, few studies on Sn-doped β-TCP scaffolds for bone tissue engineering have been reported.

Since bone defects can vary in appearance, the appearance of the scaffolds must closely match to effectively fill the defect. The porous structure of the scaffold provides space for cell growth and blood vessel formation. It also contributes to osteogenic differentiation. Therefore, the size and pore structure of the scaffold must be compatible with the bone defect repair *in vivo*. 3D printing technology can customize scaffolds with individual size and pore structure based on computer designs (Mishra et al., 2021; Ye et al., 2021; Zhang et al., 2021). The goal of this research was to fabricate a 3D-printed Sn-doped β-TCP scaffold for bone tissue applications. Moreover, we investigated the effects of Sn content on the physicochemical properties and bioactivity of the scaffold *in vitro*.

Materials and methods

Materials and reagents

β-TCP powder was purchased from Kunshan Chinese Technology New Materials Co., LTD. Sn powder was purchased from Aladdin® (Shanghai, China). The Sn-doping β-TCP scaffolds used for this work were the TCP, 1%Sn@TCP, 3%Sn@TCP and 5%Sn@TCP with nominal composition of 0 wt% Sn, 1 wt% Sn, 3 wt% Sn, and 5 wt% Sn. Tissue-Tek® OCT compound agent as a binder was purchased from Sakura Finetek United States (CA, United States). The 3D printer was assembled by ourselves, and the illustration as shown in Figure 1.

Cells

Human Umbilical Vein Endothelial Cells (HUVECs) were purchased from Cell Bank (Chinese Academy of Sciences, Shanghai, China) and cultured in endothelial cell medium (ECM, ScienCell, CA, United States). Rat bone marrow-derived

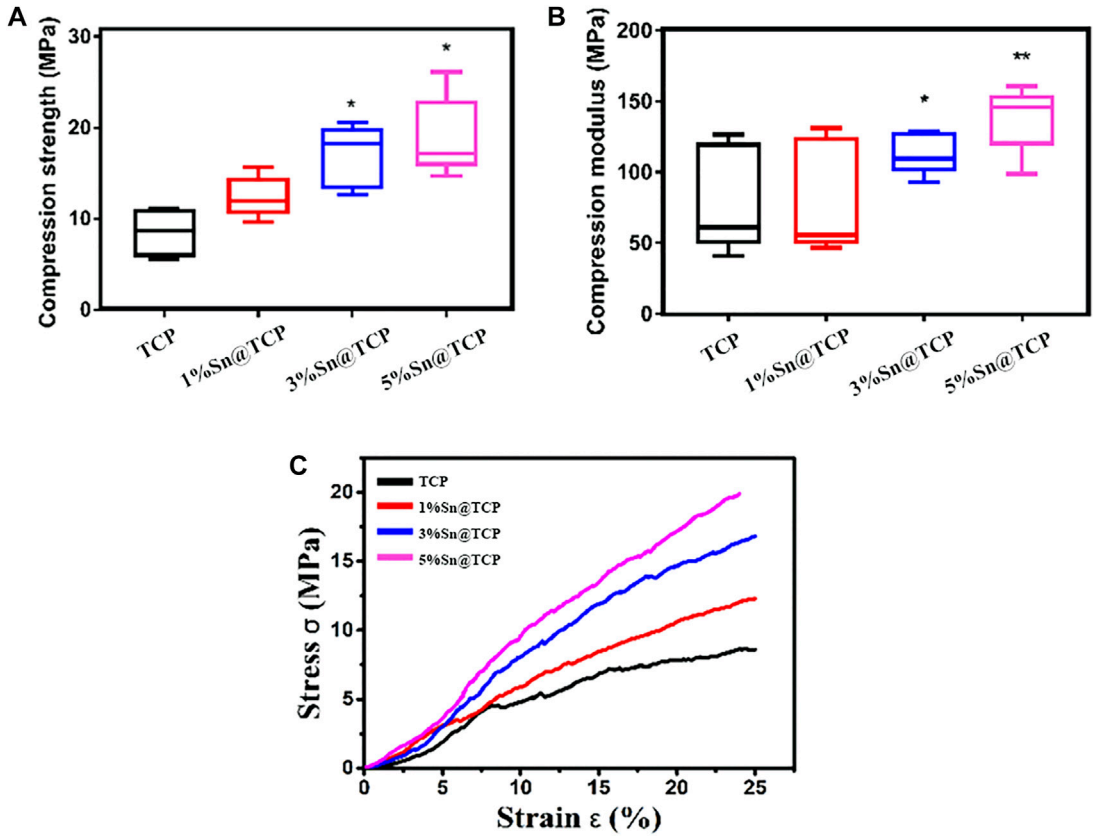

FIGURE 4
Mechanical Property of TCP scaffolds with different Sn doping. **(A)** The compression strength of TCP scaffolds with different Sn doping. **(B)** The compression modulus of TCP scaffolds with different Sn doping. **(C)** Strain-stress curve of TCP scaffolds with different Sn doping. Five scaffolds for each group (n = 5). Significance (*$p < 0.05$, **$p < 0.01$)

mesenchymal stem cell (BMSC) Isolation and Culture. 4-week-old SD rats weighing 200 ± 10 g were sacrificed by cervical dislocation and soaked in 75% ethanol for 30min. The skin, muscle and other soft tissues were obtuse separated from the tibia and femur on a super clean work table, and the tibia and femur were separated and rinsed repeatedly with PBS solution for use for several times. Sterile surgical instruments were cut off the epiphysisof long diaphysis, and only the diaphysis was preserved. DMEM low-glucose medium was extracted with a 23 G sterile syringe to slowly wash the bone marrow cavity, which showed that the contents of the bone marrow cavity oozed together with the medium. A centrifuge tube was placed at the bottom to collect the cell suspension, centrifuged at 1,000 r/min for 5 min, and the supernatant was discarded.

Design and fabricate of Sn incorporated β-TCP scaffold

Solidworks software (2014 version) was used to design the scaffold for printing. The 3D scaffold was designed as a cylindrical shape with a base area diameter of 8 mm and a height of 2 mm Simplify3D software was used to set the print parameters (printing speed: 4 mm/s, filling rate: 40%). A total of 3 g β-TCP or β-TCP@Sn (1, 3, 5% Sn doped in β-TCP) and 3 g binder were mixed for 10 min to prepare the paste for printing. The scaffolds were printed by a 3D printer assembled by ourselves. After the scaffolds were printed, there were dried in the air for 48 h and then placed inside the muffle furnace for sintering (heating rate: 10°C/min, heating temperature and time: 700°C, 900°C or 1,100°C for 3 h).

Characterization of 3D printed scaffolds

Scanning electron microscope (SEM, Sigma 300, Zeiss, Germany) was used to examine the morphology of 3D printed scaffolds. X-Ray diffraction (XRD) patterns were recorded using a D8 ADVANCE system (BRUKER, Germany) operating at 40 kV and 30 mA using a CU Kα1 radiation ($\lambda = 1.54$ Å). The XRD patterns were obtained over the range of 2θ from 5° to 90° with an angular step interval of 0.0334°. The oxidation level of Sn in Sn-doped TCP

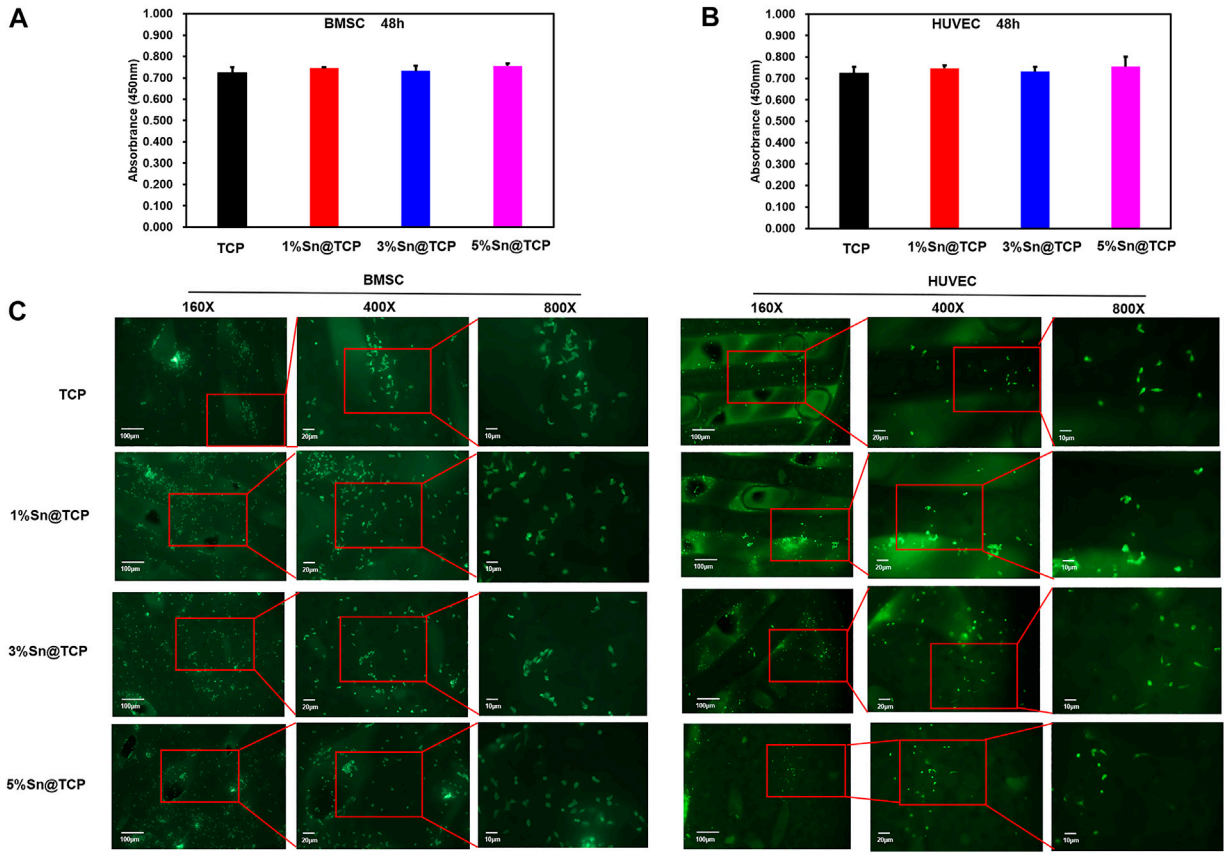

FIGURE 5
Cell growth on Sn@TCP scaffolds. **(A)** The viability of BMSC cells growth on scaffolds for 48 h. **(B)** The viability of HUVEC cells growth on scaffolds for 48 h. **(C)** The fluorescence staining of BMSC and HUVEC cells growth on scaffolds for 48 h (Magnification from ×160 to 800X, bar = 100 μm, 20μm, and 10 μm).

scaffold was determined by XPS (Thermo ESCALAB 250XI, Thermo Fisher, MA, United States). The thermal properties of the samples were studied by Thermogravimetric and differential scanning calorimetry (TG-DSC) (NETZSCH STA 449F3, Germany).

Mechanical properties

To evaluate the mechanical properties of Sn-doped, universal testing machine (Zwick/Roell Z020, Germany) was employed to measure compression strength, compression yield stress, compression modulus and stress-stain curve. The parameters are as following: test mode: compress; compression rate: 0.2 mm/min, parallel experiment: 5 times/group.

2.6 Cell proliferation on scaffolds

Cell experiments were performed by using rat BMSC primary cells and human HUVEC cell line. Each scaffold was sterilized with a autoclave followed by seeding 1×10^4 BMSC or HUVEC cells on each scaffold in a humidified incubator at 37°C and 5% CO_2. After 1–7 days in culture, WST-8 solution (10% v/v in medium) (CCK-8, Dojindo, Japan) was added to each well. After 2 h of incubation, 100 μL of each well was removed to a new 96-well plate. The absorbance value at 450 nm was measured on a multifunction microplate scanner (Tecan Infinite M200). For cell attachment, the BMSCs and HUVECs on the surface of different 3D scaffolds were visualized by Calcein-AM (Dojindo). The cell/scaffolds samples were observed under a fluorescence microscope (DMIL, LEICA, Germany).

Osteogenesis differentiation

For differentiation, ALP assay was carried out to evaluate osteogenesis ability of the BMSCs. Briefly, BMSC cells were seeded with 1×10^4 cells/well in a 24-well cell culture plate containing different scaffolds for 7 and 14 days. Then the cells were washed three times with PBS and fixed with 4%

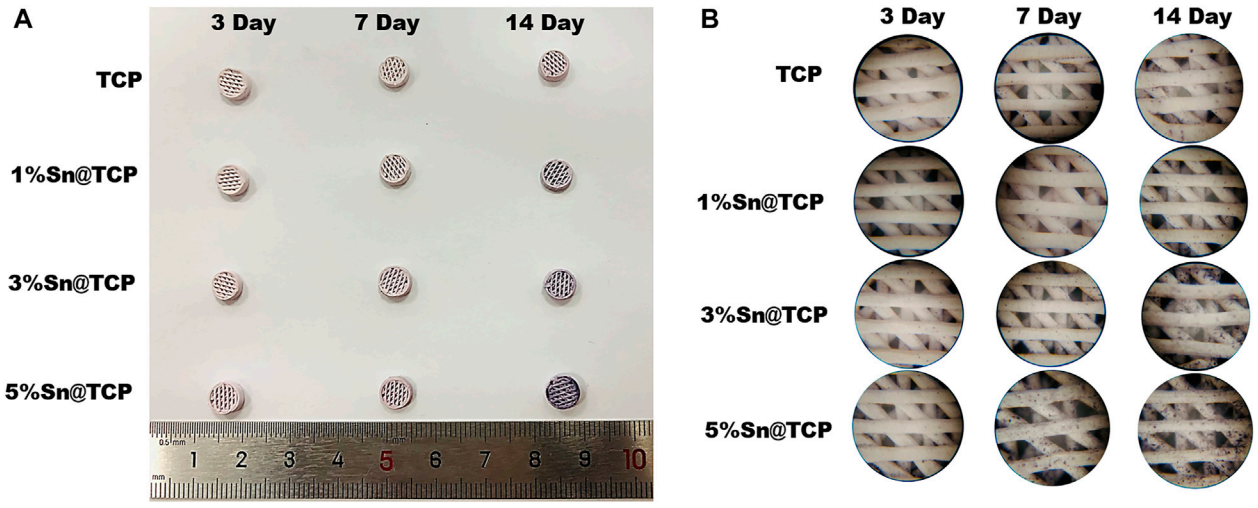

FIGURE 6
Osteoblast inducing activity of Sn@TCP scaffolds during 14 days **(A)** The photographs of ALP staining of Sn@TCP scaffolds in 3 days, 7 days and 14 days **(B)** The magnified photographs of ALP staining of Sn@TCP scaffolds in 3 days, 7 days and 14 days (Magnification 4 X).

paraformaldehyde for 15 min. The cells were rinsed gently in deionized water for 1 min. The cells were stained by alkaline-dye mixture at room temperature for 30 min and rinsed thoroughly in deionized water for 5 min. Finally, the cells on the scaffold were observed using a stereoscopic microscope (SMZ800N, Nikon, Japan).

Statistical analysis

The data were analyzed using Origin 8.0 and are presented as the mean ± standard deviation. For analysis of multiple groups, the statistic difference was evaluated by variance analysis (ANOVA one-way, Origin 8.0). A p-value of <0.05 was statistically significant.

Results and discussion

Morphology and structure of scaffolds

The Sn-doped β-TCP scaffolds were prepared by direct inject writing (DIW) 3D printing, and the fabrication process is shown in Figure 1. The β-TCP and Sn were mixed into binder agent (a water mixture of polyethylene glycol and polyvinyl alcohol, PEG + PVA) to form PEG + PVA/Sn-doped β-TCP composite material. After 3D printing and sintering, the Sn-doped β-TCP (Sn@TCP) scaffolds were constructed. The diameter and height of scaffolds and SEM images are shown in Figure 2. In Figures 2A,B, the diameter and thickness of scaffolds before sintering were 8.02 and 2.24 mm, while the diameter and thickness of scaffolds after sintering was 6.52 and 1.58 mm, respectively. The shrinkage in diameter and thickness was 18.7 and 29.5%, respectively. The appearance of the scaffolds was in accordance with the computer design.

In Figure 2C, the SEM images reveal sufficient pores in the samples after sintering, which can promote bone tissue growth. In addition, the Sn-doped materials with Sn doping display the surface of displayed angular structures on the surface. With the increase in Sn content, the angular structures of the material surface became more obvious. At a 45° angle to each filament layer, the pores were regular rhombus-shaped.

Physicochemical characterization

According to the XPS spectrum, the oxidation level of Sn in Sn@TCP was +4. The XPS spectra of 5%Sn@TCP with different sintering temperature (700°C, 900°C, and 1,100°C) indicate the same optimal sintering temperature, and an increase in the Sn3d peak after sintering at 1,100°C was observed (Figure 3A). The phase composition was verified by the Joint Committee on Powder Diffraction Standards reference patterns of β-TCP and SnO_2 (PDF No. 70–2065 and PDF No. 71–0652). The specific peaks of SnO_2 are shown in the red dotted trace in Figure 3B. As shown in Figure 3B, the peak of 5%Sn@TCP (sintering at 1,100°C) at 2θ degree around 52° increased significantly, compared with 900 and 700°C. The result indicates the optimal temperature for sintering was 1,100°C, and this is consistent with previous reports. TG-DSC analysis displayed the same trend of four groups (TCP, 1%Sn@TCP, 3%Sn@TCP,

and 5%Sn@TCP), while the weight loss percentage of TCP was the highest, compared with Sn@TCP (Figure 3C). This may result from increased oxidation of Sn during sintering. The FT-IR spectra of TCP showed a strong PO_4^{3-} peak between 1,061 and 1,024 $cm^{-}1$, corresponding to the anti-symmetric P-O stretching mode that is present in both TCP and 5Sn@TCP. The second PO_4^{3-} peak between 550 and 600 cm^{-1} corresponded to the O-P-O bending mode (Singh et al., 2016). A small peak between 800 and 900 cm^{-1} was attributed to O-Sn-O bending (Figure 3D). The mechanical properties of TCP scaffolds with different Sn contents were tested. The compression strength of 3%Sn@TCP and 5%Sn@TCP increased significantly, compared with pure TCP, as shown in Figure 4A. In addition, the compression modulus and strain-stress curve of 5%Sn@TCP enhanced significantly, compared with TCP, 1%Sn@TCP, and 3%Sn@TCP (Figures 4B,C).

Biocompatibility and osteoinduction evaluation

The cytotoxicity of TCP, 1%Sn@TCP, 3%Sn@TCP, and 5% Sn@TCP scaffolds was evaluated by examining both viability and morphologies of BMSC and HUVEC cells over 48 h. Figures 5A,B showed the cell viability of BMSC and HUVEC cells cultured in scaffolds for 48 h, compared with the negative control (TCP scaffold group). The cells cultured in 1%Sn@TCP, 3%Sn@TCP, and 5%Sn@TCP scaffolds had comparable cell viability to the negative control. This phenomenon is consistent with the reported biocompatibility of Sn-containing biomaterials. Calcein-AM staining was used to indicate the living cells and reflect the morphologies of BMSC and HUVEC cells on different scaffolds after 48 h. From Figure 5C, the number of cells stained with Calcein-AM was almost same in all of the four groups, and the cell morphology remained intact. Our results showed the Sn-doped β-TCP scaffolds exhibited good biocompatibility that was comparable to β-TCP scaffolds.

The upregulation of ALP activity indicates early mineralization of osteogenic differentiation in BMSC (Deng et al., 2017). Therefore, we chose ALP staining to evaluate the Osteogenesis differentiation activity of scaffolds. No significant difference in the level of ALP secretion was observed for β-TCP scaffolds over time. On day 14, a small number of cells secreted ALP. In contrast, Sn-doped β-TCP scaffolds showed an evident purple color, and the ALP staining of the scaffolds was dependent on the Sn content and culture duration (Figure 6).

Conclusion

In this study, we have fabricated Sn-doped TCP scaffolds successfully by DIW 3D printing and high-temperature sintering. The TCP scaffolds were doped with different ratios (0 wt% Sn, 1 wt% Sn, 3 wt% Sn, and 5 wt%) Sn and used the polyethylene glycol and polyvinyl alcohol as binder. Compared with pure TCP scaffolds, the Sn@TCP scaffolds exhibited higher mechanical properties and osteoinduction capability, presenting a Sn concentration dependent manner. Besides, the Sn@TCP scaffolds possessed good biocompatibility. Therefore, the Sn-doped TCP scaffolds satisfy the requirements for bone regeneration and represent a viable strategy for bone defect repair.

Data availability statement

The raw data supporting the conclusions of this article will be made available by the authors, without undue reservation.

Ethics statement

The animal study was reviewed and approved by Institutional Animal Care and Use Committee of Minjiang University (Approval ID: 20200821-02R).

Author contributions

HL: Conceptualization, Methodology, Writing—Original Draft, Funding acquisition. GF Methodology, Funding acquisition. JL: Investigation, Formal analysis. YT: Validation, Formal analysis. YW: Investigation, Validation. SC: Lab Resources, Funding acquisition. YZ: Lab Resources. CZ: Conceptualization, Writing—Review; Editing, Supervision, Project administration, Funding acquisition.

Funding

This work was supported by National Natural Science Foundation of China (Grant. No. 21904054, 81801849), the Natural Science Foundation of Fujian Province, China (Grant. No. 2020J05176, 2020J01865, 2022J05240), the Fujian Province Science and Technology plan, China (Grant. No. 2020Y4018), the Fund of Fujian Innovation Center of Additive Manufacturing, China (Grant. No. ZCZZ202-15).

Conflict of interest

The authors declare that the research was conducted in the absence of any commercial or financial relationships that could be construed as a potential conflict of interest.

Publisher's note

References

Deng, C. J., Yao, Q., Feng, C., Li, J., Wang, L., Cheng, G., et al. (2017). Retracted: 3D printing of bilineage constructive biomaterials for bone and cartilage regeneration. *Adv. Funct. Mat.* 27 (36), 1703117. doi:10.1002/adfm.201703117

Grado, F. D. G., Laetitia, K., Ysia, I. G., Quentin, W., Anne-Marie, M., Nadia, B. J., et al. (2018). Bone substitutes: a review of their characteristics, clinical use, and perspectives for large bone defects management. *J. Tissue Eng.* 9, 204173141877681. doi:10.1177/2041731418776819

Kang, H. J., Makkar, P., Padalhin, A. R., Lee, G. H., and Lee, B. T. (2020). Comparative study on biodegradation and biocompatibility of multichannel calcium phosphate based bone substitutes. *Mater. Sci. Eng. C* 110, 110694. doi:10.1016/j.msec.2020.110694

Kubasek, J., Vojtěcha, D., Lipov, J., and Ruml, T. (2013). Structure, mechanical properties, corrosion behavior and cytotoxicity of biodegradable Mg-X (X=Sn, Ga, In) alloys. *Mater. Sci. Eng. C* 33 (4), 2421–2432. doi:10.1016/j.msec.2013.02.005

Lynch, R. J. M., and Duckworth, R. M. (2020). Chapter 4: Microelements: Part I: Zn, Sn, Cu, Fe and I. *Monogr. Oral Sci.* 28, 32–47. doi:10.1159/000499007

Mishra, P. K., Senthil, P., Adarsh, S., and Anoop, M. S. (2021). An investigation to study the combined effect of different infill pattern and infill density on the impact strength of 3D printed polylactic acid parts. *Compos. Commun.* 24, 100605. doi:10.1016/j.coco.2020.100605

Nagy, L., Szorcsik, A., and Kovacs, K. (2000). Tin compounds in pharmacy and nutrition. *Acta Pharm. hung.* 70 (2), 53–71.

Petre, D. G., Nadar, R., Tu, Y., Paknahad, A., and Leeuwenburgh, S. C. G. (2019). Thermoresponsive brushes facilitate effective reinforcement of calcium phosphate cements. *ACS Appl. Mat. Interfaces* 11 (30), 26690–26703. doi:10.1021/acsami.9b08311

Samanta, S. K., Devi, K. B., Das, P., Mukherjee, P., Chanda, A., Roy, M., et al. (2019). Metallic ion doped tri-calcium phosphate ceramics: Effect of dynamic loading on *in vivo* bone regeneration. *J. Mech. Behav. Biomed. Mat.* 96, 227–235. doi:10.1016/j.jmbbm.2019.04.051

Shuai, C., Zhou, Y. Z., Lin, X., Yang, Y. W., Gao, C., Shuai, X., et al. (2016). Preparation and characterization of laser-melted mg-sn-zn alloys for biomedical application. *J. Mat. Sci. Mat. Med.* 28 (1), 13. doi:10.1007/s10856-016-5825-z

Singh, S. S., Roy, A., Lee, B., Banerjee, I., and Kumta, P. N. (2016). Synthesis, characterization, and *in-vitro* cytocompatibility of amorphous β-tri-calcium magnesium phosphate ceramics. *Mater. Sci. Eng. C* 67, 636–645. doi:10.1016/j.msec.2016.04.076

Tao, L., and Zhang, X. Li. (2003). Trace element tin and health. *Guangdong Trace Elem. Sci.* 10 (11), 7–12.

Vollmer, N., King, K. B., and Ayers, R. (2015). Biologic potential of calcium phosphate biopowders produced via decomposition combustion synthesis. *Ceram. Int.* 41 (6), 7735–7744. doi:10.1016/j.ceramint.2015.02.105

Wang, X., Li, J. T., Xie, M. Y., Qu, L. J., Zhang, P., and Li, X. L. (2015). Structure, mechanical property and corrosion behaviors of (HA + β-TCP)/Mg–5Sn composite with interpenetrating networks. *Mater. Sci. Eng. C* 56, 386–392. doi:10.1016/j.msec.2015.06.047

Ye, G. Y., Bi, H. J., Li, Z. L., and Hu, Y. C. (2021). Compression performances and failure modes of 3D printed pyramidal lattice truss composite structures. *Compos. Commun.* 24, 100615. doi:10.1016/j.coco.2020.100615

Zhang, X., Wang, J. L., and Liu, T. X. (2021). 3D printing of polycaprolactone-based composites with diversely tunable mechanical gradients via multi-material fused deposition modeling. *Compos. Commun.* 23, 100600. doi:10.1016/j.coco.2020.100600